C. R. Physique 13 (2012) 786–799

Contents lists available at SciVerse ScienceDirect

Comptes Rendus Physique

www.sciencedirect.com

Nanophotonics and near field / Nanophotonique et champ proche

Negative index materials and time-harmonic electromagnetic field

Matériaux d'indice négatif et champ électromagnétique harmonique en temps

Boris Gralak *, Daniel Maystre

Institut Fresnel, CNRS, Aix-Marseille université, campus de Saint Jérôme, 13397 Marseille cedex 20, France

ARTICLE INFO

Article history:
Available online 28 July 2012

Keywords:
Negative index materials
Flat lens
Evanescent waves
Macroscopic Maxwell's equations
Auxiliary field formalism

Mots-clés :
Matériaux d'indice négatif
Lentille plate
Ondes évanescentes
Équations de Maxwell macroscopiques

ABSTRACT

We study the evanescent wave's behavior on a device made of a plane interface separating vacuum from a perfect negative index material. The system is described by the macroscopic Maxwell's equations with frequency-dependent permittivity and permeability. Assuming that electromagnetic sources with sinusoidal time dependence are switched on at an initial time, we show that, as time increases, evanescent waves result in surface modes at the plane interface. The time dependence of these surface modes is oscillating but not harmonic since their amplitude linearly increases with time. As a consequence, we find that the image of a point source is not a point image. The analysis avoids any ambiguity related with causality and finite energy requirements.

RÉSUMÉ

Nous étudions le comportement des ondes évanescentes en présence d'une interface plane séparant le vide et un matériau d'indice négatif parfait. Ce système est modélisé par les équations de Maxwell macroscopiques avec des permittivité et perméabilité fonctions de la fréquence. Nous supposons que le champ électromagnétique est rayonné par des sources variant sinusoïdalement dans le temps après allumage à un instant initial. Nous montrons alors que quand le temps croît, les ondes évanescentes produisent des modes de surface sur l'interface plane. Ces modes de surfaces oscillent dans le temps mais ne sont pas harmoniques car leur amplitude croît linéairement dans le temps. Par conséquent, nous montrons que l'image d'un point source n'est plus ponctuelle. La description évite toute ambigüité relative à la causalité et l'énergie électromagnétique.

1. Introduction

In 2000, J. Pendry analyzed the behavior of evanescent waves [1] in flat lenses made of negative index material, a device proposed by V. Veselago [2]. In the case of a perfect -1 index, he found that the evanescent waves are amplified provided that the permittivity and permeability are also equal to -1. In the following, we refer to this situation as the *perfect negative index material* (PNIM). As a consequence, the flat lens becomes "perfect" since the image of a point source is a point image (see Fig. 1). This result attracted a lot of interest and rapidly, some inconsistencies appeared in the initial arguments.

* Corresponding author.
E-mail address: boris.gralak@fresnel.fr (B. Gralak).

1631-0705/$ – see front matter
http://dx.doi.org/10.1016/j.crhy.2012.04.003

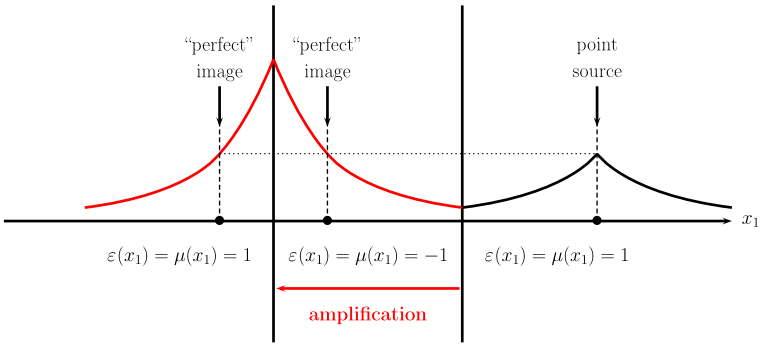

Fig. 1. The Pendry perfect lens. The ordinate of the curve shows the amplitude of an evanescent wave in space.

For example, it has been found that the resulting electromagnetic field can be infinite or that causality is not always satisfied [3–5]. Thus, it has been usually concluded that the perfect lens is an ideal case which cannot be realized in practice.

However, from our knowledge, the properties of negative index materials have always been considered in the frame of time-harmonic Maxwell's equations for monochromatic light, due to the requirement for negative permittivity and permeability to be frequency-dependent [2]. Conjecturing that the time-harmonic frame is not appropriate, we propose to consider negative index materials in the more general frame of time-dependent macroscopic Maxwell's equations. Here, our basic tool is the auxiliary field formalism introduced by A. Tip [6] and recently extended to negative index material [7]. This extension has shown that the PNIM is not in contradiction with Maxwell's equations and thus opened the possibility to study the behavior of the perfect lens. Our results lead us to the conclusion that the perfect lens is not a realistic device.

Our manuscript is organized as follows. In the next section, the problem we propose to solve is presented: the electromagnetic field is described by time-dependent macroscopic Maxwell's equations and the geometry is a single plane interface separating vacuum form a negative index material. In Section 3, we recall briefly some results and inconsistencies encountered in the time-harmonic frame. In Section 4, the auxiliary field formalism of A. Tip is presented for the situation of negative index materials. Section 5 is the key point of our approach where we propose to mimic harmonic time dependence with an electromagnetic source switched on at a given initial time. Finally, in Section 6 we show that the system can be understood as a simple RLC resonator and propose some arguments concerning the flat lens.

2. Description of the system

We assume that the behavior of the electromagnetic field in presence of negative index materials can be described by macroscopic Maxwell's equations. Denoting by $\boldsymbol{J}(\boldsymbol{x},t)$ the free current density and $\rho(\boldsymbol{x},t)$ the free charges density, these equations are [8–10]

$$\begin{aligned} &\partial_t \boldsymbol{D}(\boldsymbol{x},t) - \nabla \times \boldsymbol{H}(\boldsymbol{x},t) = -\boldsymbol{J}(\boldsymbol{x},t), \qquad \nabla \cdot \boldsymbol{D}(\boldsymbol{x},t) = \rho(\boldsymbol{x},t) \\ &\partial_t \boldsymbol{B}(\boldsymbol{x},t) + \nabla \times \boldsymbol{E}(\boldsymbol{x},t) = \boldsymbol{0}, \qquad \nabla \cdot \boldsymbol{B}(\boldsymbol{x},t) = 0 \end{aligned} \tag{1}$$

The fields $\boldsymbol{D}(\boldsymbol{x},t)$ and $\boldsymbol{H}(\boldsymbol{x},t)$ are related to $\boldsymbol{E}(\boldsymbol{x},t)$ and $\boldsymbol{B}(\boldsymbol{x},t)$ through the constitutive equations:

$$\begin{aligned} &\boldsymbol{D}(\boldsymbol{x},t) = \varepsilon_0 \boldsymbol{E}(\boldsymbol{x},t) + \boldsymbol{P}(\boldsymbol{x},t), \qquad \boldsymbol{P}(\boldsymbol{x},t) = \int_{-\infty}^{t} \mathrm{d}s\, \chi_e(\boldsymbol{x}, t-s)\boldsymbol{E}(\boldsymbol{x},s) \\ &\boldsymbol{B}(\boldsymbol{x},t) = \mu_0 \boldsymbol{H}(\boldsymbol{x},t) + \boldsymbol{M}(\boldsymbol{x},t), \qquad \boldsymbol{M}(\boldsymbol{x},t) = \int_{-\infty}^{t} \mathrm{d}s\, \chi_m(\boldsymbol{x}, t-s)\boldsymbol{H}(\boldsymbol{x},s) \end{aligned} \tag{2}$$

where ε_0 is the vacuum permittivity and μ_0 is the vacuum permeability. These constitutive equations contain the interaction of the macroscopic fields with the materials described by the polarization $\boldsymbol{P}(\boldsymbol{x},t)$ and magnetization $\boldsymbol{M}(\boldsymbol{x},t)$. Notice that they differ from the usual ones [8,9] where the magnetization $\boldsymbol{M}(\boldsymbol{x},t)$ is related to the $\boldsymbol{B}(\boldsymbol{x},t)$ field. However, in order to obtain symmetric equations, we prefer to use the equivalent equations (2) and to express Maxwell's equations in terms of the electric field $\boldsymbol{E}(\boldsymbol{x},t)$ and the magnetic field $\boldsymbol{H}(\boldsymbol{x},t)$.

The polarization and magnetization are expressed in terms of $\chi_e(\boldsymbol{x},t)$ and $\chi_m(\boldsymbol{x},t)$, the electric and magnetic susceptibilities. Causality requires these susceptibilities to vanish for negative times [8, §7.10]. As a consequence, the usual definition of permittivity $\varepsilon(\boldsymbol{x},\omega)$ and permeability $\mu(\boldsymbol{x},\omega)$ for real frequency ω, can be extended to complex number z with positive imaginary part [8, §7.10]:

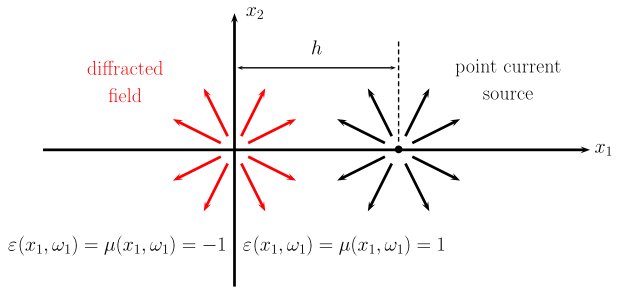

Fig. 2. The system under consideration: a point current source at a distance h from a plane interface located at $x_1 = 0$.

$$\varepsilon(\boldsymbol{x},z)=\varepsilon_0+\int_0^\infty \mathrm{d}t\,\exp[izt]\chi_e(\boldsymbol{x},t)$$
$$\mu(\boldsymbol{x},z)=\mu_0+\int_0^\infty \mathrm{d}t\,\exp[izt]\chi_m(\boldsymbol{x},t) \tag{3}$$

For $z=\omega$ purely real, the frequency dependence for permittivity and permeability is obtained from Eq. (3), which defines the dispersion relation of the materials.

We consider the situation where a single plane interface separates vacuum from a negative index material (see Fig. 2). Let (x_1,x_2,x_3) be the coordinates of vector $\boldsymbol{x}$. The plane interface is defined by $x_1=0$ and the spatial dependence of permittivity and permeability is reduced from $\boldsymbol{x}$ to x_1:

$$\begin{aligned} &x_1>0: \quad \varepsilon(x_1,z)=\varepsilon_0, \qquad \mu(x_1,z)=\mu_0\\ &x_1<0: \quad \varepsilon(x_1,z)=\varepsilon_1(z), \qquad \mu(x_1,z)=\mu_1(z)\end{aligned} \tag{4}$$

The permittivity and permeability describing the negative index material can be given by a single Lorentz resonance:

$$\frac{\varepsilon_1(z)}{\varepsilon_0}=1-\frac{\Omega_e^2}{z^2-\omega_e^2}, \qquad \frac{\mu_1(z)}{\mu_0}=1-\frac{\Omega_m^2}{z^2-\omega_m^2} \tag{5}$$

With the relations

$$\sqrt{\omega_e^2+\Omega_e^2/2}=\sqrt{\omega_m^2+\Omega_m^2/2}=\omega_1 \tag{6}$$

the material filling the half space $x_1<0$ is a PNIM for a couple of frequencies $\pm\omega_1$ since $\varepsilon_1(\pm\omega_1)/\varepsilon_0=\mu_1(\pm\omega_1)/\mu_0=-1$.

Finally, in order to study the ability of this structure to work as a perfect lens, the external (or free) current source $\boldsymbol{J}(\boldsymbol{x},t)$ is assumed to be a pure point current density along the constant vector $\boldsymbol{p}_0$:

$$\boldsymbol{J}(\boldsymbol{x},t)=g(t)\boldsymbol{j}(\boldsymbol{x}), \qquad \boldsymbol{j}(\boldsymbol{x})=\boldsymbol{p}_0\delta(\boldsymbol{x}-\boldsymbol{y}) \tag{7}$$

This point current density is located at $\boldsymbol{y}$ in the vacuum at a distance h from the interface and, without loss of generality, we can choose $\boldsymbol{y}=(h,0,0)$.

3. Time-harmonic Maxwell's equation

The time dependence of constitutive equations (2) is provided by a linear integral operator or time-convolution. This non-local relationship leads to serious difficulties to obtain directly time-dependent fields. As a consequence, a Fourier decomposition with respect to time is performed in macroscopic Maxwell's equations [8–10]. Indeed, after this transform, the constitutive equations become products of the complex and frequency-dependent dielectric permittivity and magnetic permeability (3) with Fourier-transformed fields.

The Fourier transform with respect to the time t of a field $\boldsymbol{F}(\boldsymbol{x},t)$ is

$$\hat{\boldsymbol{F}}(\boldsymbol{x},\omega)=\int_{\mathbb{R}} \mathrm{d}t\,\exp[i\omega t]\boldsymbol{F}(\boldsymbol{x},t) \tag{8}$$

and the original field is retrieved through

$$\boldsymbol{F}(\boldsymbol{x},t)=\frac{1}{2\pi}\int_{\mathbb{R}} \mathrm{d}t\,\exp[-i\omega t]\hat{\boldsymbol{F}}(\boldsymbol{x},\omega) \tag{9}$$

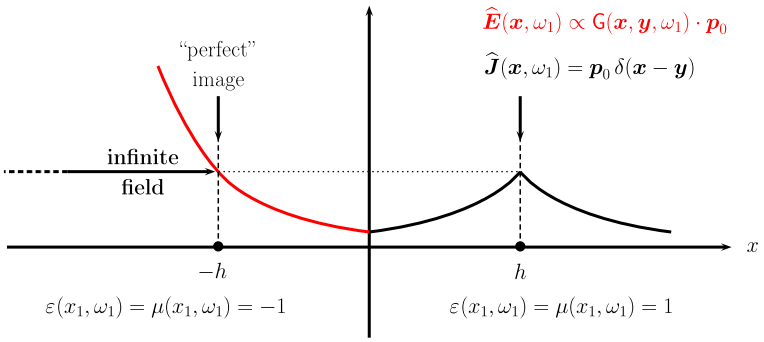

Fig. 3. Solution obtained in the frame of time-harmonic Maxwell's equations for a perfect -1 index. A "perfect" image is obtained at $x_1 = -h$. The electromagnetic field is infinite for $x_1 < -h$.

Using this Fourier transform, the constitutive equations (2) become

$$\hat{\boldsymbol{D}}(\boldsymbol{x},\omega) = \varepsilon(\boldsymbol{x},\omega)\hat{\boldsymbol{E}}(\boldsymbol{x},\omega), \qquad \hat{\boldsymbol{B}}(\boldsymbol{x},\omega) = \mu(\boldsymbol{x},\omega)\hat{\boldsymbol{H}}(\boldsymbol{x},\omega) \tag{10}$$

and the macroscopic Maxwell's equations lead to time-harmonic Maxwell's equations satisfied by the Fourier-transformed electric and magnetic fields:

$$\begin{aligned} i\omega\varepsilon(\boldsymbol{x},\omega)\hat{\boldsymbol{E}}(\boldsymbol{x},\omega) &= -\nabla\times\hat{\boldsymbol{H}}(\boldsymbol{x},\omega) + \hat{\boldsymbol{J}}(\boldsymbol{x},\omega) \\ i\omega\mu(\boldsymbol{x},\omega)\hat{\boldsymbol{H}}(\boldsymbol{x},\omega) &= \nabla\times\hat{\boldsymbol{E}}(\boldsymbol{x},\omega) \end{aligned} \tag{11}$$

The substitution of the magnetic field amplitude leads to an equation in terms of the Helmholtz operator for the electric field amplitude:

$$\begin{aligned} \mathsf{H}_e(\omega)\hat{\boldsymbol{E}}(\boldsymbol{x},\omega) &= \omega^2\varepsilon(\boldsymbol{x},\omega)\hat{\boldsymbol{E}}(\boldsymbol{x},\omega) - \nabla\times\frac{1}{\mu(\boldsymbol{x},\omega)}\nabla\times\hat{\boldsymbol{E}}(\boldsymbol{x},\omega) \\ &= -i\omega\hat{\boldsymbol{J}}(\boldsymbol{x},\omega) \end{aligned} \tag{12}$$

Replacing the source amplitude by its expression $\hat{\boldsymbol{J}}(\boldsymbol{x},\omega) = \hat{g}(\omega)\boldsymbol{p}_0\delta(\boldsymbol{x}-\boldsymbol{y})$, the electric field amplitude is proportional to the Green's function:

$$\hat{\boldsymbol{E}}(\boldsymbol{x},\omega) = -i\omega\hat{g}(\omega)\mathsf{G}(\boldsymbol{x},\boldsymbol{y},\omega)\cdot\boldsymbol{p}_0 \tag{13}$$

where the Green's function is defined as the solution of

$$\mathsf{H}_e(\omega)\mathsf{G}(\boldsymbol{x},\boldsymbol{y},\omega) = \delta(\boldsymbol{x}-\boldsymbol{y}) \tag{14}$$

Finally, with time dependence $g(t) = \sin[\omega t]$, we can write the source $\boldsymbol{J}(\boldsymbol{x},t)$ as the real part of the quantity $i\exp[-i\omega t]\boldsymbol{j}(\boldsymbol{x})$ which leads to $\hat{g}(\omega) = 2i\pi$. Denoting be "Re" the real part, the harmonic real electric field is

$$\hat{\boldsymbol{E}}(\boldsymbol{x},\omega) = \mathrm{Re}\big\{\omega\exp[-i\omega t]\mathsf{G}(\boldsymbol{x},\boldsymbol{y},\omega)\cdot\boldsymbol{p}_0\big\} \tag{15}$$

The calculation of the Green's function for a PNIM at frequency ω_1 in the case of the flat lens can be found in the literature [4,11]. We start from this result and then let the second interface go toward minus infinity. The obtained result for the evanescent waves is represented in Fig. 3. It shows a total transmission at the interface and an amplification of the transmitted wave. As a result, the amplitude of this wave at $x_1 = -h$ is exactly the same than the one on the source at $x_1 = h$. Thus the image at $x_1 = -h$ can be considered as perfect. However, for values of x_1 below $-h$, the amplitude of the transmitted wave is still amplified and the corresponding electric field is infinite.

At this stage, the solution generally considered in the literature is to add small absorption γ to the negative index material. In this case, the present system is similar to the negative index slab considered in [3], where the two interfaces become uncoupled for a slab thick enough. It can be checked that the reflection coefficient is proportional to the inverse of the parameter γ, and the corresponding solution shows the presence of a surface mode with amplitude proportional to γ^{-1} (see Fig. 4). This solution has now a finite energy but, on the other hand, the image at $x_1 = -h$ is not perfect. More important, the limit of the solution when the small absorption γ tends towards zero does not exist. This behavior is in contradiction with usual situations in physics where the introduction of a small absorption leads, at the limit, to an acceptable solution.

To conclude this section, we think that the solutions obtained in the frame of harmonic Maxwell's equations are not satisfactory: in particular we pointed out some problems related with infinite energy or the low absorption limit. In addition, some arguments based on causality [5] have been reported in the literature.

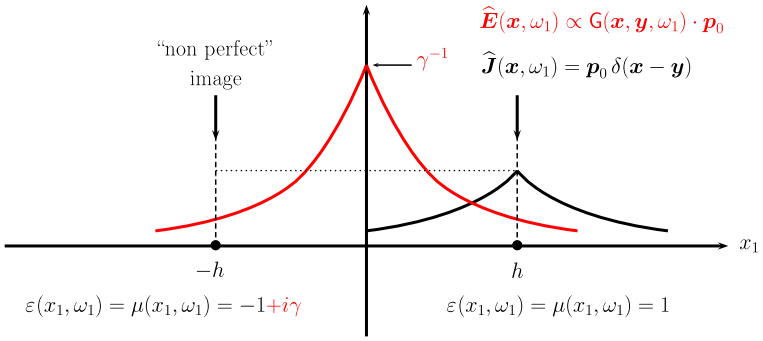

Fig. 4. Solution obtained in the frame of time-harmonic Maxwell's equations for a non-perfect -1 index with low absorption γ. The obtained image at $x_1 = -h$ is "non-perfect". The electromagnetic field is finite. (For interpretation of the references to color in this figure, the reader is referred to the web version of this article.)

4. Auxiliary field formalism of A. Tip

The auxiliary field formalism is based on the definition of suitable auxiliary fields [6,7]. They are defined in such a way that their "energy" compensates exactly the electromagnetic energy absorbed by the materials. As a consequence, the vector $F(\boldsymbol{x},\omega,t)$ which contains the electromagnetic field and the auxiliary fields has conserved "energy" and thus satisfies a unitary time-evolution equation

$$\partial_t F(t) = -i\mathsf{K}F(t) \tag{16}$$

where K is a self-adjoint operator independent of time. In this frame, we are led to a well-known description often found in quantum mechanics [12], providing an elegant way to solve Maxwell's equations. In particular, the time-dependent solution without free sources is obviously $F(t) = \exp[-i\mathsf{K}(t-t_0)]F(t_0)$ and the general inhomogeneous solution is provided thanks to the Duhamel's formula. Finally, the original electric field $\boldsymbol{E}(\boldsymbol{x},t)$ is retrieved applying to the field $F(t)$ the projector P_e:

$$\boldsymbol{E}(\boldsymbol{x},t) = \mathsf{P}_e F(\boldsymbol{x},\omega,t) \tag{17}$$

In the following of this section, the construction of the auxiliary field formalism of A. Tip is briefly presented [6,7]. The solution in the particular case of a monochromatic external excitation in the presence of negative index materials is reported in the next section.

The auxiliary field formalism starts from the set of linear macroscopic Maxwell's equations (1) without the free current and charge densities:

$$\begin{aligned}
&\partial_t \boldsymbol{D}(\boldsymbol{x},t) - \nabla\times\boldsymbol{H}(\boldsymbol{x},t) = \boldsymbol{0}, \qquad \nabla\cdot\boldsymbol{D}(\boldsymbol{x},t) = 0\\
&\partial_t \boldsymbol{B}(\boldsymbol{x},t) + \nabla\times\boldsymbol{E}(\boldsymbol{x},t) = \boldsymbol{0}, \qquad \nabla\cdot\boldsymbol{B}(\boldsymbol{x},t) = 0
\end{aligned} \tag{18}$$

The auxiliary fields $\boldsymbol{A}_e(\boldsymbol{x},\omega,t)$ and $\boldsymbol{A}_m(\boldsymbol{x},\omega,t)$ are defined from the electric and magnetic fields respectively:

$$\begin{aligned}
\boldsymbol{A}_e(\boldsymbol{x},\omega,t) &= \int_{-\infty}^{t} \mathrm{d}s \exp\bigl[-i\omega(t-s)\bigr]\boldsymbol{E}(\boldsymbol{x},s)\\
\boldsymbol{A}_m(\boldsymbol{x},\omega,t) &= \int_{-\infty}^{t} \mathrm{d}s \exp\bigl[-i\omega(t-s)\bigr]\boldsymbol{H}(\boldsymbol{x},s)
\end{aligned} \tag{19}$$

Next the following couple of positive functions is introduced:

$$\begin{aligned}
\nu_e(\boldsymbol{x},\omega) &= \nu_e(\boldsymbol{x},-\omega) = \frac{\omega\,\mathrm{Im}\,\varepsilon(\boldsymbol{x},\omega)}{2\pi} \geqslant 0\\
\nu_m(\boldsymbol{x},\omega) &= \nu_m(\boldsymbol{x},-\omega) = \frac{\omega\,\mathrm{Im}\,\mu(\boldsymbol{x},\omega)}{2\pi} \geqslant 0
\end{aligned} \tag{20}$$

These two functions are directly related to the fundamental quantity called "*oscillator strength*" [10, §82]. Initially defined from the permittivity and permeability, these functions can be related as well to the susceptibilities:

$$\partial_t \chi_e(\boldsymbol{x},t) = \int_{\mathbb{R}} \mathrm{d}\omega \exp[-i\omega t]\nu_e(\boldsymbol{x},\omega) = \int_{\mathbb{R}} \mathrm{d}\omega \cos[\omega t]\nu_e(\boldsymbol{x},\omega)$$
$$\partial_t \chi_m(\boldsymbol{x},t) = \int_{\mathbb{R}} \mathrm{d}\omega \exp[-i\omega t]\nu_m(\boldsymbol{x},\omega) = \int_{\mathbb{R}} \mathrm{d}\omega \cos[\omega t]\nu_m(\boldsymbol{x},\omega) \tag{21}$$

Then, the derivative with respect to time of the polarization becomes

$$\begin{aligned}
\partial_t \boldsymbol{P}(\boldsymbol{x},t) &= \partial_t \int_{-\infty}^{t} \mathrm{d}s\, \chi_e(\boldsymbol{x},t-s)\boldsymbol{E}(\boldsymbol{x},s) \\
&= \chi_e(\boldsymbol{x},0)\boldsymbol{E}(\boldsymbol{x},t) + \int_{-\infty}^{t} \mathrm{d}s\, \partial_t \chi_e(\boldsymbol{x},t-s)\boldsymbol{E}(\boldsymbol{x},s) \\
&= \int_{-\infty}^{t} \mathrm{d}s \int_{\mathbb{R}} \mathrm{d}\omega \exp\big[-i\omega(t-s)\big]\nu_e(\boldsymbol{x},\omega)\boldsymbol{E}(\boldsymbol{x},s) \\
&= \int_{\mathbb{R}} \mathrm{d}\omega\, \nu_e(\boldsymbol{x},\omega) \int_{-\infty}^{t} \mathrm{d}s \exp\big[-i\omega(t-s)\big]\boldsymbol{E}(\boldsymbol{x},s) \\
&= \int_{\mathbb{R}} \mathrm{d}\omega\, \nu_e(\boldsymbol{x},\omega)\boldsymbol{A}_e(\boldsymbol{x},\omega,t)
\end{aligned} \tag{22}$$

and similarly for the magnetization:

$$\partial_t \boldsymbol{M}(\boldsymbol{x},t) = \int_{\mathbb{R}} \mathrm{d}\omega\, \nu_m(\boldsymbol{x},\omega)\boldsymbol{A}_m(\boldsymbol{x},\omega,t) \tag{23}$$

Thus the derivative with respect to time of all the fields is given by:

$$\begin{aligned}
\partial_t \boldsymbol{E}(\boldsymbol{x},t) &= \nabla \times \boldsymbol{H}(\boldsymbol{x},t) - \int_{\mathbb{R}} \mathrm{d}\omega\, \nu_e(\boldsymbol{x},\omega)\boldsymbol{A}_e(\boldsymbol{x},\omega,t) \\
\partial_t \boldsymbol{H}(\boldsymbol{x},t) &= -\nabla \times \boldsymbol{E}(\boldsymbol{x},t) - \int_{\mathbb{R}} \mathrm{d}\omega\, \nu_m(\boldsymbol{x},\omega)\boldsymbol{A}_m(\boldsymbol{x},\omega,t) \\
\partial_t \boldsymbol{A}_e(\boldsymbol{x},\omega,t) &= \boldsymbol{E}(\boldsymbol{x},t) - i\omega\boldsymbol{A}_e(\boldsymbol{x},\omega,t) \\
\partial_t \boldsymbol{A}_m(\boldsymbol{x},\omega,t) &= \boldsymbol{H}(\boldsymbol{x},t) - i\omega\boldsymbol{A}_m(\boldsymbol{x},\omega,t)
\end{aligned} \tag{24}$$

Let us denote by $F(\boldsymbol{x},\omega,t)$ the vector containing the electromagnetic field and the auxiliary fields:

$$F(\boldsymbol{x},\omega,t) = \begin{bmatrix} \boldsymbol{E}(\boldsymbol{x},t) \\ \boldsymbol{H}(\boldsymbol{x},t) \\ \boldsymbol{A}_e(\boldsymbol{x},\omega,t) \\ \boldsymbol{A}_m(\boldsymbol{x},\omega,t) \end{bmatrix} \tag{25}$$

According to this definition, the projector P_e, providing the electric field from the total field (17), is

$$\mathsf{P}_e = \begin{bmatrix} 1 & 0 & 0 & 0 \\ 0 & 0 & 0 & 0 \\ 0 & 0 & 0 & 0 \\ 0 & 0 & 0 & 0 \end{bmatrix} \tag{26}$$

The total field satisfies the time-evolution equation (16) where

$$\mathsf{K} = \begin{bmatrix} 0 & i\nabla\times & -i\int_{\mathbb{R}} \mathrm{d}\omega\, \nu_e(\boldsymbol{x},\omega) & 0 \\ -i\nabla\times & 0 & 0 & -i\int_{\mathbb{R}} \mathrm{d}\omega\, \nu_m(\boldsymbol{x},\omega) \\ 1 & 0 & \omega & 0 \\ 0 & 1 & 0 & \omega \end{bmatrix} \tag{27}$$

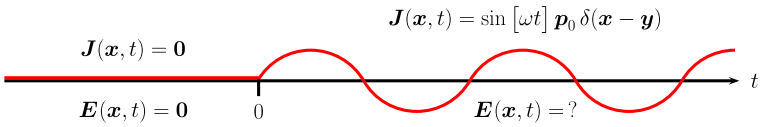

Fig. 5. The source $\boldsymbol{J}(\boldsymbol{x},t)$ is switched on at $t=0$ and then monochromatic for later times.

The operator K is self-adjoint when acting on the suitable Hilbert space of square integrable functions with the norm

$$\begin{aligned}\left\|F(t)\right\|^2 &= \int_{\mathbb{R}^3} \mathrm{d}\boldsymbol{x}\left|\boldsymbol{E}(\boldsymbol{x},t)\right|^2 + \int_{\mathbb{R}^3} \mathrm{d}\boldsymbol{x}\left|\boldsymbol{H}(\boldsymbol{x},t)\right|^2 \\ &+ \int_{\mathbb{R}^3} \mathrm{d}\boldsymbol{x} \int_{\mathbb{R}} \mathrm{d}\omega\, \nu_e(\boldsymbol{x},\omega)\left|\boldsymbol{A}_e(\boldsymbol{x},\omega,t)\right|^2 \\ &+ \int_{\mathbb{R}^3} \mathrm{d}\boldsymbol{x} \int_{\mathbb{R}} \mathrm{d}\omega\, \nu_m(\boldsymbol{x},\omega)\left|\boldsymbol{A}_m(\boldsymbol{x},\omega,t)\right|^2 \end{aligned} \tag{28}$$

Note that the above quantity actually defines a norm thanks to the fact that the functions $\nu_e(\boldsymbol{x},\omega)$ and $\nu_m(\boldsymbol{x},\omega)$ are always positive. Also, this quantity is the usual conserved energy [8, §6.7] when there are no external (or free) current and charge densities.

5. Monochromatic external excitation

In this section, we consider an external sinusoidal source switched on at the initial time $t=0$ (see Fig. 5) with the spatial dependence (7):

$$\boldsymbol{J}(\boldsymbol{x},t)=g(t)\,\boldsymbol{j}(\boldsymbol{x}), \qquad g(t)=\theta(t)\sin[\omega t], \qquad \boldsymbol{j}(\boldsymbol{x})=\boldsymbol{p}_0\delta(\boldsymbol{x}-\boldsymbol{y}) \tag{29}$$

where θ is the step function [$\theta(t)=1$ for $t>0$ and $\theta(t)=0$ for $t<0$]. We stress that the present approach is very close to the experimental conditions. In particular, it can be expected that, after some transition period, a permanent monochromatic behavior is achieved and can be compared with the time-harmonic solution.

With the auxiliary field formalism, the equation to solve is:

$$\partial_t F(t) = -i\mathsf{K}F(t) - S(t) \tag{30}$$

where $S(t)$ is the four-component vector with the current density $\boldsymbol{J}(\boldsymbol{x},t)$ as first component and null vectors elsewhere, which thus satisfies $\mathsf{P}_e S(t)=S(t)$ (note that P_e is the projector upon the electric fields (17)). Thanks to the Duhamel's formula (also denominated by "variation de la constante" in French),

$$F(t)=\exp[-i\mathsf{K}t]F(0) - \int_0^t \mathrm{d}s\exp\left[-i\mathsf{K}(t-s)\right]S(s) \tag{31}$$

Assuming that the field is produced by the source S switched on at the initial time $t=0$, the field $F(t)$ is vanishing for negative time and $F(0)=0$. In addition, it allows to define the Laplace-transformed field for complex number z with positive imaginary part:

$$\hat{F}(z)=\int_0^\infty \mathrm{d}t\exp[izt]F(t) = -\int_0^\infty \mathrm{d}t\exp[izt]\int_0^t \mathrm{d}s\exp\left[-i\mathsf{K}(t-s)\right]S(s) \tag{32}$$

Bearing in mind that $S(s)$ vanishes for negative times and performing the change $s\to t-s$ yields:

$$\begin{aligned}\hat{F}(z) &= -\int_0^\infty \mathrm{d}t\exp[izt]\int_{-\infty}^t \mathrm{d}s\exp\left[-i\mathsf{K}(t-s)\right]S(s) \\ &= -\int_0^\infty \mathrm{d}t\exp[izt]\int_0^\infty \mathrm{d}s\exp[-i\mathsf{K}s]S(t-s)\end{aligned}$$

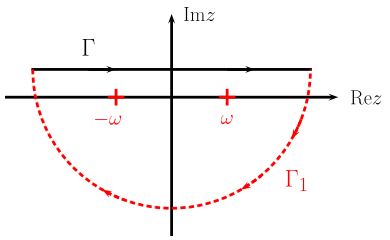

Fig. 6. Schematic representation of the continuation of the integral path Γ to pick up the poles contributions. The integral over the dashed arc Γ_1 in the lower half plane of complex numbers z is vanishing for $t \to \infty$.

$$
\begin{aligned}
&= -\int_0^\infty \mathrm{d}s \exp[izs] \exp[-i\mathsf{K}s] \int_0^\infty \mathrm{d}t \exp\bigl[iz(t-s)\bigr] S(t-s) \\
&= -\int_0^\infty \mathrm{d}s \exp\bigl[i(z-\mathsf{K})s\bigr] \int_{-s}^\infty \mathrm{d}t \exp[izt] S(t) \\
&= -\int_0^\infty \mathrm{d}s \exp\bigl[i(z-\mathsf{K})s\bigr] \int_0^\infty \mathrm{d}t \exp[izt] S(t) \\
&= \frac{i}{\mathsf{K}-z} \hat{S}(z)
\end{aligned}
\tag{33}
$$

Notice that here, we used that the operator K is self-adjoint which ensures for the inverse of $[\mathsf{K}-z]$ to be well-defined provided the number z has a non-zero imaginary part. Next the original time-dependent field is retrieved from

$$
F(t) = \frac{1}{2i\pi} \int_\Gamma \mathrm{d}z \exp[-izt] \hat{F}(z) = \frac{1}{2i\pi} \int_\Gamma \mathrm{d}z \exp[-izt] \frac{1}{z-\mathsf{K}} \hat{S}(z) \tag{34}
$$

where Γ is a line parallel to the real axis in the upper half plane of complex numbers z. Denoting (a little bit improperly from a mathematical view point) $\boldsymbol{j}(\boldsymbol{x})$ as a vector similar to $S(t)$ with three additional null vector components, the Laplace transform of the source leads to

$$
\hat{S}(z) = \int_0^\infty \mathrm{d}t \sin[\omega t] \mathsf{P}_e \boldsymbol{j}(\boldsymbol{x}) = \frac{1}{2} \left[\frac{1}{z+\omega} - \frac{1}{z-\omega} \right] \mathsf{P}_e \boldsymbol{j}(\boldsymbol{x}) \tag{35}
$$

and the field $F(t)$ is given by the integral

$$
\mathsf{I}(t) = \frac{1}{4i\pi} \int_\Gamma \mathrm{d}z \exp[-izt] \frac{1}{z-\mathsf{K}} \left[\frac{1}{z+\omega} - \frac{1}{z-\omega} \right] \tag{36}
$$

This calculation can be achieved in closed form by deforming the path from Γ to Γ_1 so that it passes underneath the poles at $\pm\omega$. Then, it can be shown that the integral over the path Γ_1 vanishes when the time t tends toward infinity, so that the integral (36) reduces to the poles contributions: schematically, it is possible to close the loop from the path Γ in order to pick up the poles (Fig. 6). Assuming that $[z-\mathsf{K}]^{-1}$ is analytic, we have:

$$
\mathsf{I}(t) \underset{t\to\infty}{\approx} \frac{1}{2} \left[\frac{\exp[-i\omega t]}{\omega - \mathsf{K}} + \frac{\exp[+i\omega t]}{\omega + \mathsf{K}} \right] \tag{37}
$$

where $[\omega \pm \mathsf{K}]^{-1}$ has to be understood as the limit when $\eta \to 0$ of $[\omega + i\eta \pm \mathsf{K}]^{-1}$. Hence,

$$
\boldsymbol{E}(\boldsymbol{x}, t) = \mathsf{P}_e F(t) \underset{t\to\infty}{\approx} \mathsf{P}_e \frac{1}{2} \left[\frac{\exp[-i\omega t]}{\omega - \mathsf{K}} + \frac{\exp[+i\omega t]}{\omega + \mathsf{K}} \right] \mathsf{P}_e \boldsymbol{j}(\boldsymbol{x}) \tag{38}
$$

It can be shown that the "electric field coefficient" of the inverse $[z-\mathsf{K}]^{-1}$ is precisely the inverse of the electric Helmholtz operator [7, Appendix B]:

$$
\mathsf{P}_e [z-\mathsf{K}]^{-1} \mathsf{P}_e = z \mathsf{R}_e(z), \qquad \mathsf{R}_e(z)^{-1} = \mathsf{H}_e(z) = z^2 \varepsilon(\boldsymbol{x}, z) - \nabla \times \frac{1}{\mu(\boldsymbol{x}, z)} \nabla \times \tag{39}
$$

As a consequence, denoting by $\mathsf{G}(\boldsymbol{x},\boldsymbol{y},z)$ the Green's function associated with the electric Helmholtz operator and $\mathsf{G}(\boldsymbol{x},\boldsymbol{y},z)^\dagger$ its hermitian adjoint (as a matrix), we obtain

$$\mathsf{P}_e[z-\mathsf{K}]^{-1}\mathsf{P}_e\,\boldsymbol{j}(\boldsymbol{x}) = z\mathsf{R}_e(z)\,\boldsymbol{j}(\boldsymbol{x}) = z\mathsf{G}(\boldsymbol{x},\boldsymbol{y},z)\cdot\boldsymbol{p}_0 = z\mathsf{G}(\boldsymbol{x},\boldsymbol{y},-\bar{z})^\dagger\cdot\boldsymbol{p}_0 \tag{40}$$

which leads to:

$$\begin{aligned}\boldsymbol{E}(\boldsymbol{x},t) = \mathsf{P}_e F(t) &\underset{t\to\infty}{\approx} \frac{1}{2}\big\{\omega\mathsf{G}(\boldsymbol{x},\boldsymbol{y},\omega)\exp[-i\omega t] + \omega\mathsf{G}(\boldsymbol{x},\boldsymbol{y},\omega)^\dagger\exp[i\omega t]\big\}\cdot\boldsymbol{p}_0\\ &= \operatorname{Re}\big\{\omega\exp[-i\omega t]\mathsf{G}(\boldsymbol{x},\boldsymbol{y},\omega)\cdot\boldsymbol{p}_0\big\}\end{aligned} \tag{41}$$

Here we precisely get the well-known result obtained in the time-harmonic frame (see Section 3). However, it has to be noticed that it is obtained under the assumption for the inverse $[z-\mathsf{K}]^{-1}$ to be analytic. Especially, in the case of a single interface separating vacuum and a PNIM, this inverse has precisely a pole for evanescent waves at the frequencies $\pm\omega_1$ [7]. In this context, the inverse can be written

$$\frac{1}{z-\mathsf{K}} = \frac{\mathsf{L}_+(z)}{z-\omega_1} + \frac{\mathsf{L}_-(z)}{z+\omega_1} \tag{42}$$

with $\mathsf{L}_+(z)$ and $\mathsf{L}_-(z)$ analytic, and the integral $\mathsf{I}(t)$ becomes

$$\mathsf{I}(t) = \frac{1}{4i\pi}\int_\Gamma \mathrm{d}z\exp[-izt]\left[\frac{\mathsf{L}_+(z)}{z-\omega_1} + \frac{\mathsf{L}_-(z)}{z+\omega_1}\right]\left[\frac{1}{z+\omega} - \frac{1}{z-\omega}\right] \tag{43}$$

Consequently, the operator $\mathsf{I}(t)$ for $t\to\infty$ is now provided by the contribution of four poles. Similarly, the Green's function associated with the electric Helmholtz operator can be written in term of analytic functions $\mathsf{A}_+(\boldsymbol{x},\boldsymbol{y},z)$ and $\mathsf{A}_-(\boldsymbol{x},\boldsymbol{y},z)$ [these functions are actually the kernel of the analytic operators $\mathsf{L}_+(z)$ and $\mathsf{L}_-(z)$]:

$$\mathsf{G}(\boldsymbol{x},\boldsymbol{y},z) = \frac{1}{z}\left[\frac{\mathsf{A}_+(\boldsymbol{x},\boldsymbol{y},z)}{z-\omega_1} + \frac{\mathsf{A}_-(\boldsymbol{x},\boldsymbol{y},z)}{z+\omega_1}\right] \tag{44}$$

The resulting electric field is

$$\begin{aligned}\boldsymbol{E}(\boldsymbol{x},t) &\underset{t\to\infty}{\approx} \operatorname{Re}\frac{\mathsf{A}_+(\boldsymbol{x},\boldsymbol{y},\omega)\exp[-i\omega t] - \mathsf{A}_+(\boldsymbol{x},\boldsymbol{y},\omega_1)\exp[-i\omega_1 t]}{\omega-\omega_1}\cdot\boldsymbol{p}_0\\ &\quad - \operatorname{Re}\frac{\mathsf{A}_+(\boldsymbol{x},\boldsymbol{y},-\omega)\exp[-i(-\omega)t] - \mathsf{A}_+(\boldsymbol{x},\boldsymbol{y},\omega_1)\exp[-i\omega_1 t]}{(-\omega)-\omega_1}\cdot\boldsymbol{p}_0\end{aligned} \tag{45}$$

Here, we definitely find a result which cannot be found in the frame of time-harmonic Maxwell's equations. Indeed, the electric field has contributions oscillating at the excitation frequency ω and also contributions oscillating at the frequency ω_1!

Finally, we can examine the behavior of this solution when the excitation frequency ω is tending towards the frequency ω_1. For example, the first term in expression (45) will lead when $\omega\to\omega_1$ to the derivative

$$\operatorname{Re}\left\{\frac{\partial}{\partial\omega}\mathsf{A}_+(\boldsymbol{x},\boldsymbol{y},\omega)\exp[-i\omega t]\right\}_{\omega=\omega_1} = \operatorname{Re}\left\{\frac{\partial\mathsf{A}_+}{\partial\omega}(\boldsymbol{x},\boldsymbol{y},\omega_1)\exp[-i\omega_1 t] - it\mathsf{A}_+(\boldsymbol{x},\boldsymbol{y},\omega_1)\exp[-i\omega_1 t]\right\} \tag{46}$$

Since this expression is valid for large time only, the second term clearly dominates and the time-dependent electric field is given, when $\omega\to\omega_1$, by:

$$\boldsymbol{E}(\boldsymbol{x},t) \underset{t\to\infty}{\approx} \operatorname{Re}\big\{-it\exp[-i\omega_1 t]\mathsf{A}_+(\boldsymbol{x},\boldsymbol{y},\omega_1)\cdot\boldsymbol{p}_0\big\} \tag{47}$$

Again, the time dependence of the electric field is oscillating but not harmonic and its amplitude is increasing linearly with time. As regards the spatial dependence, thanks to causality, it is actually the same than in the time-harmonic frame with low absorption γ. Indeed, causality imposes the imaginary part of the permittivity and permeability to be positive and, in the same time, it allows to consider complex frequency z with positive imaginary part 3: in fact, adding small absorption γ is equivalent of adding a small imaginary part η to ω. Thus the behavior obtained for evanescent waves is the same than the one presented in Fig. 4, except that the inverse of absorption γ^{-1} has to be replaced by t. It implies that electromagnetic energy is accumulating around the interface separating vacuum and the negative index material (see Fig. 7). Since the amplitudes of the evanescent waves increase with time, they have no reason to be simultaneously equal to the ones of the punctual excitation at $\boldsymbol{y}=(h,0,0)$, and thus the image of the point source in the PNIM is certainly not perfect. In the case the excitation frequency ω is not equal to the resonance frequency ω_1, the expression (45) shows that the electric field is the sum of two time-harmonic waves. The first wave, oscillating at the frequency ω, is the same than the one with low absorption, and thus yields a non-perfect image governed by a low absorption γ proportional to $\omega-\omega_1$. As to the second wave, oscillating at the frequency ω_1, it does not have propagative components and is superimposed with the first wave. As a result, a non-perfect image is expected.

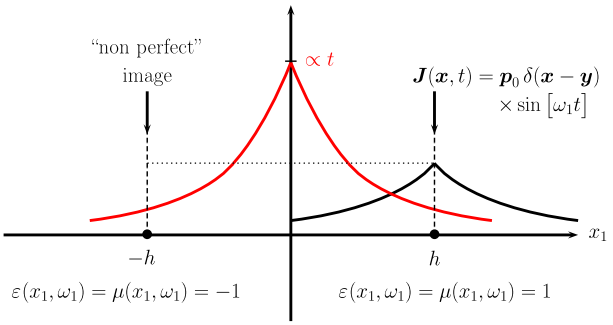

Fig. 7. Time-dependent solution of Maxwell's equations for a perfect -1 index. A "non-perfect" image is obtained at $x_1 = -h$.

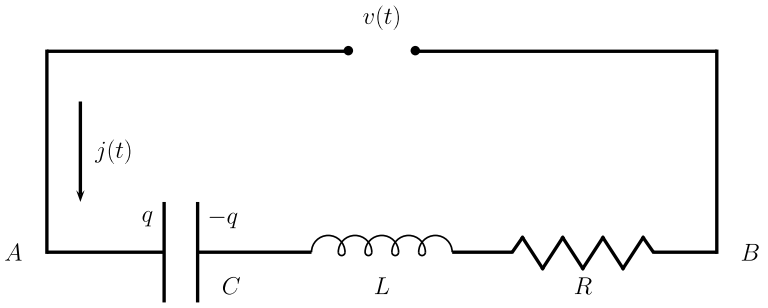

Fig. 8. The RLC resonant circuit.

6. Discussion

6.1. A simple model: the RLC resonator

The preceding sections have shown the interest of the description of the negative index materials in terms of poles of the field in the complex plane of z. The existence of these poles shows that basically, these materials are able to provoke resonance phenomena. The aim of this section is to show on a very simple example that the linear increase of the field with time described by Eq. (47) constitutes a general phenomenon encountered in lossless resonant devices.

We consider the RLC circuit shown in Fig. 8. A voltage $v(t) = V_A - V_B$ generates in the RLC circuit a current $j(t)$ which can be written, using the convention of Fig. 8:

$$v(t) = \frac{q}{C} + L\frac{\mathrm{d}j}{\mathrm{d}t} + Rj \tag{48}$$

with q charge of the capacitor. Taking the derivative of Eq. (48) yields:

$$L\frac{\mathrm{d}^2 j}{\mathrm{d}t^2} + R\frac{\mathrm{d}j}{\mathrm{d}t} + \frac{j}{C} = \frac{\mathrm{d}v}{\mathrm{d}t} \tag{49}$$

We first consider the harmonic case, thus we can use the complex notation and we know that the complex amplitude $\hat{\jmath}$ of the current is given by $\hat{\jmath} = \hat{v}/Z$, with $\hat{v}$ the complex amplitude of the voltage v, the impedance Z of the RLC circuit being given by

$$Z = R + i\frac{LC\omega^2 - 1}{C\omega} \tag{50}$$

When R does not vanish, $\hat{\jmath}$ remains bounded but if R tends to zero, Z tends to zero at the resonance frequency ω_1 such that $LC\omega_1^2 = 1$, thus at this resonance frequency the current is infinite. From an intuitive point of view, this is not surprising since the energy provided by the generator cannot be dissipated. We deduce that a harmonic solution for the current does not exist at resonance.

Now let us suppose that the voltage begins at $t = 0$ and is given by:

$$v(t) = \theta(t)\sin[\omega t] \tag{51}$$

In addition, we consider the case which makes problems, i.e. $R = 0$. We deduce from Eq. (49) that:

$$L\frac{\mathrm{d}^2 j}{\mathrm{d}t^2} + \frac{j}{C} = \omega\theta(t)\cos[\omega t] \tag{52}$$

In order to solve this linear differential equation of the second order with a right-hand member, we need two conditions at $t = 0$. First, assuming that $v(t)$ is bounded, the presence of an inductance entails the continuity of the current $j(t)$, thus

$$j(0^+) = 0 \tag{53}$$

Second, since $j(t)$ is bounded and vanishes at $t = 0^+$, the voltage q/C on the capacitor vanishes as well. Since the voltage is continuous $[v(0^+) = 0]$, we deduce that the voltage on the inductance vanishes:

$$L\frac{\mathrm{d}j}{\mathrm{d}t}(0^+) = v(0^+) = 0 \tag{54}$$

It can be deduced from these two initial conditions that Eq. (49) is satisfied in the sense of distributions.

The solution of Eq. (52) can be expressed as the sum of the general solution of the differential equation without right-hand member and a particular solution of the differential equation with right-hand member. The general solution j_1 of the differential equation without right-hand member can be written for $t > 0$ in the form:

$$j_1(t) = a\cos[\omega_1 t] + b\sin[\omega_1 t] \tag{55}$$

with ω_1 resonance frequency given by $LC\omega_1^2 = 1$. A particular solution of the differential equation with right-hand member can be expressed in the form:

$$j_2(t) = a'\cos[\omega t] + b'\sin[\omega t] \tag{56}$$

and introducing j_2 in Eq. (52) leads to:

$$a' = \frac{\omega C}{1 - LC\omega^2} = \frac{C}{L(\omega_1^2 - \omega^2)}, \qquad b' = 0 \tag{57}$$

Now, writing that the solution $j_1 + j_2$ must satisfy the initial conditions at $t = 0$ [Eqs. (53) and (54)] leads, after straightforward calculations to $a = -a'$, $b = -b'$. We deduce the expression of the current:

$$j(t) = \frac{C}{L(\omega_1^2 - \omega^2)}\big\{\cos[\omega t] - \cos[\omega_1 t]\big\}\theta(t) \tag{58}$$

As in the case of negative index materials, the solution for $\omega \neq \omega_1$ contains both frequencies ω and ω_1. When ω is equal to ω_1, the right-hand side of Eq. (58) is undetermined since both $\cos[\omega t] - \cos[\omega_1 t]$ and $\omega_1^2 - \omega^2$ vanish. However, it is possible to calculate the limit of the expression by noticing that $\cos[\omega t] - \cos[\omega_1 t] \approx t(\omega_1 - \omega)\sin[\omega_1 t]$. Finally, we get:

$$\text{if } \omega \to \omega_1, \quad j(t) \to \frac{1}{2L}t\sin[\omega_1 t]\theta(t) \tag{59}$$

This very simple result shows that, as in the case of a negative index material, the solution oscillates at frequency ω_1 with a modulus which linearly increases with time. We conclude that this behavior is general in resonance phenomena in lossless devices, and many other examples could be found, for example in mechanics with the lossless harmonic oscillator. It is very interesting to notice that in lossless devices, the classical hypothesis which states that the output in a resonator excited by a sinusoidal signal starting at $t = -\infty$ is the limit when $t \to \infty$ of the output when the same device is excited by a sinusoidal signal starting at $t = 0$ fails. In fact, it exists in addition to the harmonic output at the excitation frequency an output at the resonance frequency which obviously has crucial consequences.

6.2. The simple model applied to the negative index system

The model presented above (Section 6.1) invites to check if the simple technique used to analyze the LC circuit can be applied to the PNIM system. In this aim, the time-harmonic Maxwell's equations are considered with a sinusoidal current density. After a Fourier decomposition with respect to the space variables x_2 and x_3, the component $U = E_2$ of the electric field is the solution of the Helmholtz equation

$$\frac{\partial}{\partial x_1}\frac{1}{\mu(x_1,\omega)}\frac{\partial}{\partial x_1}U + \left[\omega^2\varepsilon(x_1,\omega) - \frac{k_3^2}{\mu(x_1,\omega)}\right]U = \omega\cos[\omega t]\delta(x_1 - h) \tag{60}$$

By analogy with the LC circuit, a solution U of this equation can be written as the sum of the solution U_1 without right-hand member and a particular solution U_2 with right-hand member. The general solution U_1 satisfying the finite energy criterion is

$$U_1(x_1, k_3, t) = \big\{a_1\cos[\omega_1 t] + b_1\sin[\omega_1 t]\big\}\exp\Big[-\sqrt{k_3^2 - \omega_1^2\varepsilon_0\mu_0}|x_1|\Big] \tag{61}$$

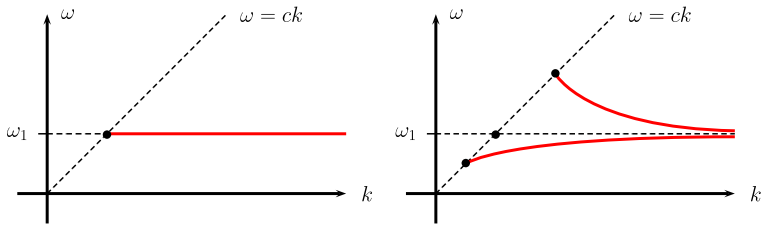

Fig. 9. Dispersion law for the single interface (left part) and the flat lens (right part): $c = \sqrt{\varepsilon_0\mu_0}$ is the light speed in vacuum.

with $k_3^2 - \omega_1^2\varepsilon_0\mu_0 \geqslant 0$, thanks to the PNIM condition $\varepsilon(\omega_1)/\varepsilon_0 = \mu(\omega_1)/\mu_0 = -1$. This solution is a surface mode, localized at the plane interface separating the PNIM from vacuum, and with harmonic time dependence at frequency ω_1. Next the particular solution is given by the one-dimensional Green's function $G(x_1, h, k_3, \omega)$:

$$U_2(x_1, k_3, \omega_1) = G(x_1, h, k_3, \omega)\omega\cos[\omega t] \tag{62}$$

The Green's function above is well-defined for $\omega \neq \omega_1$ and, when the excitation frequency ω tends to ω_1, its profile is similar to the one depicted in Fig. 4 with $\gamma = \omega_1 - \omega$.

At this stage, it has to be noted that the two solutions U_1 and U_2 have different profiles, and that the two degrees of freedom, provided by the coefficients a_1 and b_1, do not make possible to match any arbitrary initial condition. In particular, it is not possible to assume that the electric field vanishes at some initial time. This situation shows that the simple technique used for the LC circuit cannot be rigorously applied to the PNIM situation.

However, at the limit when ω tends to ω_1, the amplitude of the diffracted part in the Green's function (the red part in Fig. 4) tends to infinity as $1/(\omega_1 - \omega)$. In these conditions, it may be considered that the solution U_2 resembles the surface mode U_1 for $k_3^2 - \omega_1^2\varepsilon_0\mu_0 \geqslant 0$:

$$U_2(x_1, k_3, \omega) \underset{\omega\to\omega_1}{\approx} U_0\frac{\omega\cos[\omega t]}{\omega_1 - \omega}\exp\left[-\sqrt{k_3^2 - \omega_1^2\varepsilon_0\mu_0}|x_1|\right] \tag{63}$$

where U_0 is a constant. Now, it is possible to find a solution $U = U_1 + U_2$ which satisfies the initial condition $U = 0$ and $\partial U/\partial t = 0$ at $t = 0$ and thus vanishes for negative times:

$$U \underset{\omega\to\omega_1}{\approx} U_0\omega\frac{\cos[\omega t] - \cos[\omega_1 t]}{\omega_1 - \omega}\theta(t)\exp\left[-\sqrt{k_3^2 - \omega_1^2\varepsilon_0\mu_0}|x_1|\right] \tag{64}$$

Finally, using that $\cos[\omega t] - \cos[\omega_1 t] \approx t(\omega_1 - \omega)\sin[\omega_1 t]$, this solution becomes

$$U \underset{\omega\to\omega_1}{\approx} U_0\omega_1 t\sin[\omega_1 t]\theta(t)\exp\left[-\sqrt{k_3^2 - \omega_1^2\varepsilon_0\mu_0}|x_1|\right] \tag{65}$$

Again, it is found that the solution has amplitude linearly with time. While this result provided by the simple technique is certainly useful, it is pointed that the reasoning on which it is based is not rigorous. This situation shows that the auxiliary field formalism is a unique tool to consider rigorously the time-dependent Maxwell's equations.

6.3. The flat lens

In the case of the single interface separating vacuum form the PNIM, it can be shown easily that there exists a surface mode oscillating at the frequency ω_1 for all evanescent waves. For instance, the reflection coefficient for *s*-polarization, which can be written for evanescent waves

$$r_0(z) = m(z)\frac{1}{z^2 - \omega_1^2}, \qquad k_3^2 - \omega_1^2\varepsilon_0\mu_0 \geqslant 0 \tag{66}$$

with $m(z)$ is analytic around ω_1 [7], presents poles at $z = \pm\omega_1$. The resulting dispersion law shows a horizontal line at frequency ω_1 (see the left part of Fig. 9). Considering the flat lens as a system of two plane interfaces, we can expect that it will present two modes resulting from the interaction of the two surface modes supported by the interfaces. Indeed, the expression of the reflection coefficient on a PNIM layer of thickness h,

$$r(z) = r_0(z)\frac{1 - \exp[2ih\zeta(z)]}{1 - r_0^2(z)\exp[2ih\zeta(z)]}, \qquad \zeta(z) = \sqrt{z^2\varepsilon_1(z)\mu_1(z) - k_3^2} \tag{67}$$

shows that each pole at $z = \pm\omega_1$ splits into a couple:

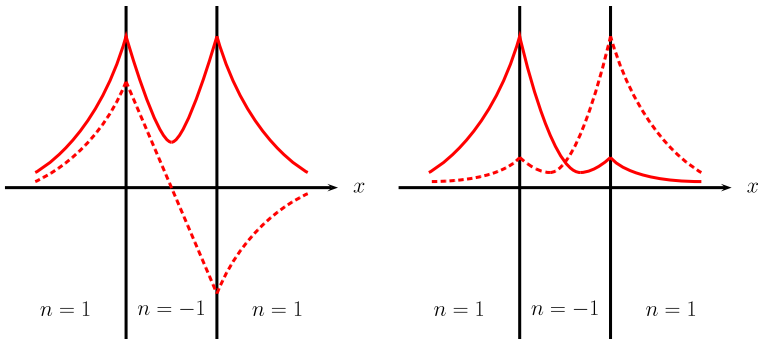

Fig. 10. Left part: the modes supported by the flat lens; a symmetric one (continuous line) and an anti-symmetric one (discontinuous line). Right part: example of combination of the flat lens modes; one mode is confined on the left interface (continuous line) while the second mode is confined on the right interface (discontinuous line).

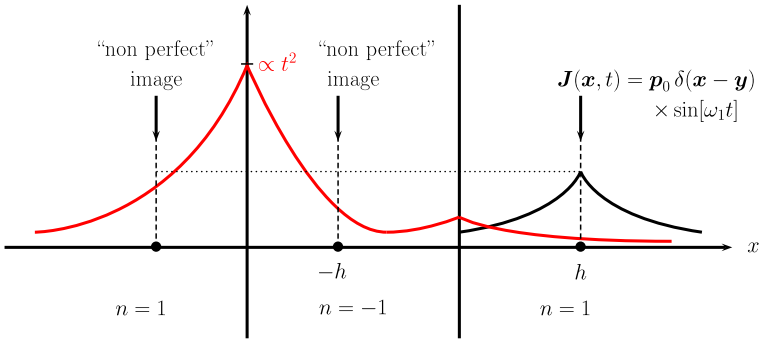

Fig. 11. Time-dependent solution of Maxwell's equations for a perfect -1 index flat lens. A "non-perfect" image is expected.

$$\frac{1}{r(z)} = 0 \quad \Longrightarrow \quad \frac{1}{r_0(z)} = \frac{z^2 - \omega_1^2}{m(z)} = \pm \exp\bigl[ih\zeta(z)\bigr]$$
$$\Longrightarrow \quad z \approx \omega_1 \pm \frac{m(\omega_1)}{2\omega_1} \exp\bigl[ih\zeta(\omega_1)\bigr] \tag{68}$$

This expression, which solves the degeneracy, shows that these two modes are located above and below the original horizontal line at ω_1 on the dispersion law (see the right part of Fig. 9). One of these modes is symmetric while the second one is anti-symmetric with respect to the horizontal plane of symmetry of the device (see Fig. 10 and the recent papers of R. Collin [13] and J. Pendry [14]). The sum (difference) of these two modes is constructive (destructive) on the first interface and destructive (constructive) on the second one.

Thus it is possible to approach the result obtained by Pendry, represented in Fig. 1, with a combination of the flat lens modes. However, it has to be noticed that, from our analysis, the amplitudes of these modes are now governed by the superposition of three poles on the complex plane: a couple of poles corresponding to the degeneracy plus a pole corresponding to the excitation. The resulting amplitudes are then expected to be proportional to the square t^2 of time (see Fig. 11 and [13]). Thus it is found that the amplitudes of the evanescent waves, increasing with time, have no reason to be simultaneously equal to the ones of the punctual excitation at $\boldsymbol{y} = (h, 0, 0)$. A a consequence, it can be expected that the image of a point source through the -1 index flat lens should not be perfect.

Acknowledgements

Adriaan Tip is gratefully acknowledged for fruitful exchanges and discussions.

This work was partly supported by the project FANI (Grant No. ANR-07-NANO-038-03) funded by the Agence nationale de la recherche.

References

[1] J.B. Pendry, Negative refraction makes a perfect lens, Phys. Rev. Lett. 85 (18) (2000) 3966–3969.
[2] V.G. Veselago, The electrodynamics of substances with simultaneously negative values of ε and μ, Sov. Phys. Usp. 10 (4) (1968) 509–514.
[3] N. Garcia, M. Nieto-Vesperinas, Left-handed materials do not make a perfect lens, Phys. Rev. Lett. 88 (2002) 207403.
[4] D. Maystre, S. Enoch, Perfect lenses made with left-handed materials: Alice's mirror? J. Opt. Soc. Am. A 21 (2004) 122.

[5] I. Stockman, Criterion for negative refraction with low optical losses from a fundamental principle of causality, Phys. Rev. Lett. 98 (2007) 177404.
[6] A. Tip, Linear absorptive dielectric, Phys. Rev. A 57 (1998) 4818–4841.
[7] B. Gralak, A. Tip, Macroscopic Maxwell's equations and negative index materials, J. Math. Phys. 51 (2010) 052902.
[8] J.D. Jackson, Classical Electrodynamics, 3rd edition, Wiley, New York, 1998.
[9] J.G. Van Bladel, Electromagnetic Fields, 2nd edition, John Wiley and Sons, 2007.
[10] L.D. Landau, E.M. Lifshitz, L.P. Pitaevskiĭ, Electrodynamics of Continuous Media, Courses of Theoretical Physics, vol. 8, 2nd edition, Elsevier, Oxford, 1984.
[11] D. Maystre, S. Enoch, B. Gralak, G. Tayeb, Metamaterials: from microwaves to the visible region, Comptes Rendus Physique 6 (2005) 693.
[12] C. Cohen-Tannoudji, B. Diu, F. Laloë, Mécanique Quantique, Hermann, 1973.
[13] R.E. Collin, Frequency dispersion limits resolution in Veselago lens, J. PIER B 19 (2010) 233–261.
[14] W.H. Wee, J.B. Pendry, Universal evolution of perfect lenses, Phys. Rev. Lett. 106 (2011) 165503.